*Article*

# A Dynamic Analysis of the Cycloid Disc Stress-Strain State

Milos Matejic [1], Mirko Blagojevic [1], Aleksandar Disic [1], Marija Matejic [2], Vladimir Milovanovic [1] and Ivan Miletic [1,*]

1 Faculty of Engineering, University of Kragujevac, Sestre Janjic 6, 34000 Kragujevac, Serbia
2 Faculty of Technical Sciences, University of Pristina with Temporary Settled in Kosovska Mitrovica, Knjaza Milosa 7, 38220 Kosovska Mitrovica, Kosovo
* Correspondence: imiletic@kg.ac.rs; Tel.: +381-64-670-55-67

**Featured Application: In this study, an original approach to the dynamic analysis of cycloid disc stress-strain state is proposed, which provides a very accurate picture of dynamic processes in cycloid drives.**

**Abstract:** The problem of internal forces that occur on the cycloid disc during the cycloid speed reducer operation so far has not been considered in a way that reflects its actual workloads and stresses in the cycloid disc itself. This paper presents a dynamic analysis of the stress-strain state of a cycloid disc by using experimental and numerical methods. The following cases of meshing are presented in the paper: a single-tooth, double-tooth, and triple-tooth meshing of the cycloid disc and the ring gear. The cycloid disc was chosen for this study because it is one of the main elements and the most critical element of the cycloid speed reducer. An experimental physical model of the cycloid disc and the meshing elements of the cycloid speed reducer was made based on a previously performed 3D CAD model. The numerical analysis of the stress-strain state of the cycloid disc was performed with the identically defined external load using the transient stress method. The paper presents a comparative analysis of the experimental and numerical results, which gives a solid insight into what is happening in the cycloid disc during the cycloid speed reducer operation. The experimental and simulation results both give the results with a deviation between 3% and 15%. After the detailed analyses, it is shown that the most critical element of cycloid speed reducer are output rollers, which need further study.

## 1. Introduction

Over the last few decades, cycloid speed reducers have found a wide application in engineering practice. They are generally used as reducers, while their applications as multipliers or two-way power transmission systems have not been sufficiently studied yet. Cycloid speed reducers have a great number of good performance characteristics, such as a wide range of transmission ratios, extremely compact design, low noise and vibration, lightweight concerning the torque they transmit, ability to transmit high torques, reliable operation under intensive dynamic loads, high efficiency, etc. All these good operating characteristics together with a good price range, give them an advantage over conventional speed reducers. These gear trains have found application in robots, satellites, manipulation devices, crane machines, large industrial mixers, conveyors, and renewable energy sources (wind generators, mini hydro power plants).

The cycloid speed reducer force analysis and stresses in reducer elements caused by internal forces is a very complex task. For that reason, the cycloid speed reducer elements are often over-dimensioned, considering the possible problems that can be encountered in the cycloid speed reducer operation. The first analysis of the cycloid speed reducer internal

forces was performed by Kudrijavcev in his book *Planetary Gear Train* [1]. His model was further improved by Lehmann [2] in his doctoral thesis. Malhorta and Parameswaran [3] developed a detailed model for determining the forces on all the elements of the cycloid speed reducer, which they later used to calculate the efficiency. The further published research about cycloid reducer dynamic analysis can be divided into two main groups: the papers that deal mainly with analytical models and simulations and the papers with dynamic simulations compared with experimental testing. One of the first papers from the first group of research was performed by Thube and Bobak [4], showing the detailed dynamic simulation in CAD software of a cycloid speed reducer without a theoretical background. On the other hand, Kniazeva and Goman [5] gave the analytical method of excitation force creation and its transformation into internal reducer forces. Furthermore, Wang et al. [6] analyzed sliding speed in cycloid speed reducers. Li [7] did a static analysis of the stress state in cycloid discs interacting with other reducer meshing elements. Hsieh [8,9] did both simulation and experimental analysis in classic cycloid speed reducers and non-pin wheel cycloid speed reducers, comparing their results. Shen et al. [10] did a dynamic analysis of cycloid speed reducers with special attention to their vibrations. Other authors in this field [11–17] did various dynamic simulations of cycloid speed reducer working using different software for its analysis, such as SolidWorks, ANSYS, MSC NASTRAN, etc. Two papers [18–20] in this field have been different because they described the simulation of contact stresses in cycloid discs all along their width. One of the most influential factors in the cycloid speed reducer dynamic is its machining and manufacturing tolerances [21]. Very accurate research about forces and stress calculation was performed by Efremenkov et al. [22], which can be used as a starting point for further experimental analyses.

Papers from the second group of papers related to cycloid reducer dynamics involve investigations with experimental testing. These papers were not published often because of the experiments' complexity and their costs. One of the first papers related to cycloid reducer dynamics was written by Hsieh [8], and the part related to the experiment was conducted in an open power circuit. In that research, the output torque was measured in two types of reducers: classic cycloid reducer and non-pin wheel concept. Another publication that had an experiment was by Kumar et al. [23]. After analysis in ANSYS, they found that the existing mechanism of the cycloid speed reducer was a critical part and they performed an experiment on the real model. The vibration analysis, numerically and experimentally, was conducted by Chen and Yang [24]. The same group of authors also performed one more experiment with a classic type of cycloid speed reducer and a new proposed model [25]. In that experiment, they used an accelerometer on the reducer output to have insight into the output shaft starting and stopping. They also conducted additional research with the same model, where they performed vibration analyses and oscillation modes [25]. Recent research in this field [26] shows the proposed design of a cycloid speed reducer with experimental verification of its functioning.

The authors of this research also have a background in this field, both theoretical and experimental papers. A solid foundation in the field of cycloid reducer research was conducted by Blagojevic [27] in his doctoral thesis. Furthermore, Blagojevic et al. [28] set up the single-stage cycloid reducer dynamic model, solved in MATLAB. In later research, a group of authors [29] analyzed the new concept of a two-stage cycloid reducer that uses one cycloid disc instead of two per transmission stage. This research uses an experiment of cycloid disc static loading. Blagojevic et al. [30] conducted FEM and experimental analyses on one cycloid disc from a cycloid speed reducer in static conditions. Interesting research by Blagojevic and a group of authors [31] was conducted similarly to [7], but NASTRAN was used for the solving software. For the new concept of a cycloid speed reducer presented in Blagojevic's Ph.D. thesis, a complete dynamic model has been given in the paper [32]. In another paper [33], the authors gave complete static analyses for a particular cycloid speed reducer with forces calculated on each reducer element. Blagojevic et al. [34] investigate the influence of friction forces on cycloid drive efficiency. In that paper, they show that

friction forces can greatly impact cycloid drive operation due to decreased lubrication in case of oil leakage, lubricant decreased properties during operation, etc.

During dynamic load conditions, power transmissions must keep their stability, precision, and endurance. Therefore, examining cycloid speed reductions in dynamic load conditions is very significant. As can be noticed, in the available literature, most papers have analytical and numerical results. Few papers have an experiment. Most of the shown experiments in the available literature are conducted under static load conditions. The problem with static load conditions is that a physical process in the actual working conditions of the cycloidal drive is not simulated properly. Some of the dynamic experiments shown in the literature review only give output values of torque or output of acceleration. These experiments do not give complete insight into what is happening in the cycloid speed reducer during meshing in working conditions. Thus far, the experimental dynamic loading of the cycloid disc in laboratory conditions is not published because the examination methodology is very complex. In this paper, the authors will present a new approach to cycloid disc dynamic testing as well as cycloid disc mesh elements (output pin and meshing tooth). The testing was conducted both experimentally and numerically.

The rest of the paper is structured as follows: Section 2 presents the loading cases of the cycloid disc and its theoretical background. Section 3 presents experimental testing. In Section 4, the numerical testing was shown. Section 5 deals with the discussion of the results. At the end of the paper, in Section 6, conclusions are drawn.

## 2. Theoretical Model of the Cycloid Disc Loading

This paper studies a classic single-stage cycloid speed reducer with two cycloid discs shown in Figure 1. The paper is orientated in cycloid disc dynamic analyses and elements that interact with it during the cycloid speed reducer operation.
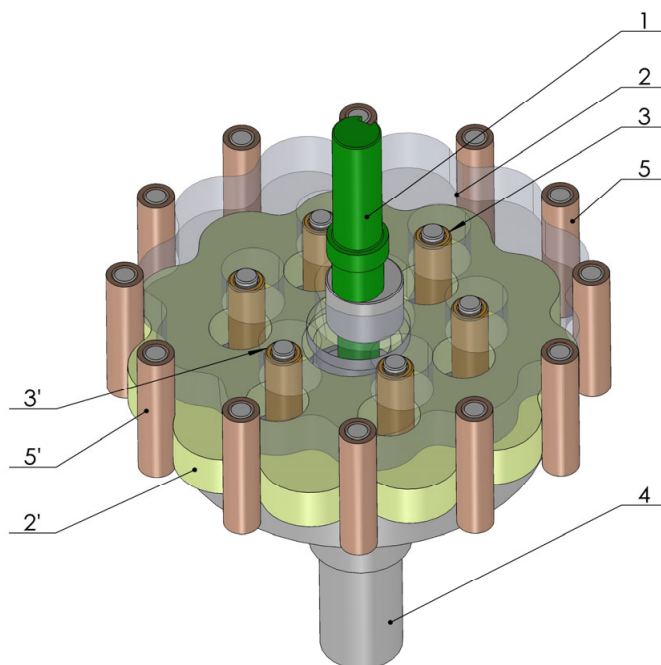


**Figure 1.** 3D model of a classic single-stage cycloid speed reducer: 1—input shaft; 2 and 2'—cycloid discs; 3 and 3'—output rollers; 4—exiting mechanism, and 5 (5')—ring gear rollers.

A cycloid speed reducer is a very complex system from the aspect of its geometry as well as from the aspect of its kinematic and dynamic structure. In order to perform the analysis, it is necessary to know the loads that act on the cycloid disc as the main element of the cycloid speed reducer. Figure 2 shows the forces acting on the cycloid disc during meshing. They are the following [1,2]:
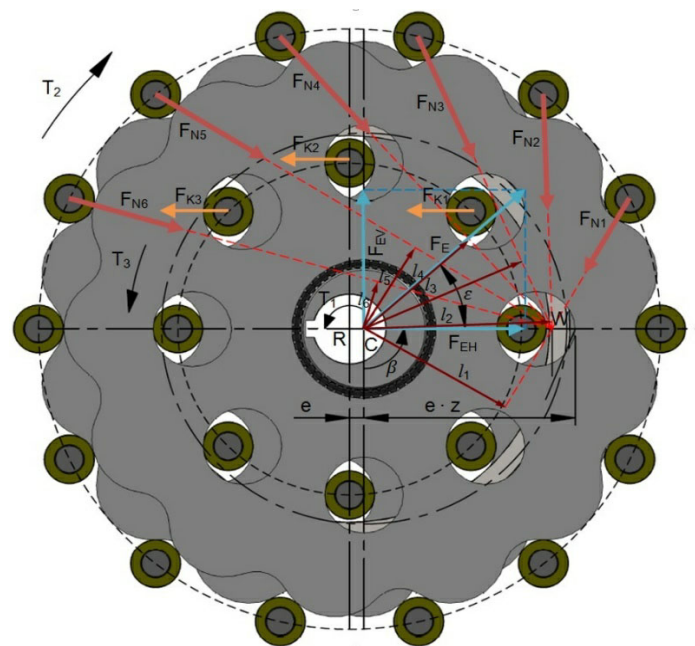
**Figure 2.** Forces on the cycloid disc [35].

- $F_E$—eccentric cam force (the force where the vertical component $F_{EV}$ generates the drive torque $T_1$ on the cycloid disc due to its eccentric rotation),
- $F_N$—normal force at the current contact point of the cycloid disc tooth and the stationary ring gear roller (normal force),
- $F_K$—normal force at the current contact point of the output roller and the opening in the cycloid disc (output force).

The torques due to which these forces occur are:

- $T_1$—drive torque of the cycloid disc,
- $T_2$—torque on the ring gear,
- $T_3$—output torque of the cycloid disc.

From Figure 2, it is evident that this is a statically indeterminate system. The only known force is the vertical component of the eccentric cam force $F_{EV}$. Kudrijavcev defined the first procedure for calculation of the forces acting on the cycloid disc in his book *Planetary Gear Train* in 1966 [1]. Both Kudrijavcev and Lehmann [2], as pioneers in this field, analyzed the ideal case of the cycloid disc meshing with other elements of the cycloid speed reducer. In this case, there are no clearances between the teeth of the cycloid disc and the rollers of the stationary ring gear, hence the assumption that half of the teeth of the cycloid disc transfer the load simultaneously. This is obviously not the case in real operating conditions. In reality, clearances exist for many reasons: as the result of manufacturing faults, to facilitate assembly and disassembly for maintenance purposes, and to enable adequate lubrication, among other reasons. Kudrijavcev's procedure for calculating the normal force occurring in the contact of the cycloid disc and the stationary ring gear roller is described in great detail in the literature [1]. In this paper, only the basic expressions are presented in order to help understand the calculation of the normal force in experimental and numerical analyses.

The normal force on the *i*-th roller is calculated based on Equation (1):

$$F_{Ni} = F_{Nmax} \cdot \frac{l_i}{r_1} \tag{1}$$

where $F_{Nmax}$—is the maximum value of the normal force, $l_i$—is the normal distance from the center of the cycloid disc to the corresponding normal force (Figure 2), $r_1$—is the radius of the stationary circle [1].

Since the output torque of the cycloid disc $T_3$ is given by Equation (2):

$$T_3 = F_{\text{Nmax}} \cdot r_1 \cdot z_2 \cdot \frac{\sum\limits_i l_i^2}{r_1^2 \cdot z_2} \tag{2}$$

Having solved Equation (2), the maximum value of the normal force can be calculated as in Equation (3):

$$F_{\text{Nmax}} = \frac{4 \cdot T_3}{r_1 \cdot z_2} \tag{3}$$

where $z_2$ is the number of the rollers of the stationary ring gear.

The size of the clearances between the ring gear and the cycloid disc is directly related to the number of the ring gear rollers meshing with the cycloid disc. The larger the clearances, the smaller the number of the meshed teeth of the cycloid disc and the rollers of the ring gear. In this paper, three types of meshing were analyzed: triple-tooth, double-tooth, and single-tooth meshing. The single-tooth meshing is the most unfavorable type because only one tooth of the cycloid disc and one roller of the ring gear is meshing. The cycloid disc of the single-stage cycloid speed reducer (Figure 2) used in this paper has the following characteristics:

- Input power: $P_{\text{in}} = 5.5$ kW;
- Input number of revolutions: $n_{\text{in}} = 1450$ min$^{-1}$;
- Gear ratio: $u_r = 11$;
- Eccentricity $e = 4$ mm.

Numerical and experimental analyses were performed for all three types of meshing and for three different loads: 50% of $F_{\text{Nmax}}$, 100% of $F_{\text{Nmax}}$, and 150% of $F_{\text{Nmax}}$. The overload of 150% of $F_{\text{Nmax}}$ is taken into account in cases of shock loads or increased friction loads due to decreased lubrication occurring during the cycloid drive operation. Based on Equation (1), the normal forces were calculated as a function of the driving angle from the moment the cycloid disc teeth entered the mesh up to the moment they exited the mesh. Until the cycloid disc teeth enter the mesh, the normal meshing force equals zero. This procedure was carried out for all three types of meshing: single-tooth, double-tooth, and triple-tooth meshing. Based on the obtained values for the normal force, an approximate function of the normal force was obtained by function fitting and used in the experimental and numerical analyses. Approximate functions of the normal force are given in Table 1.

**Table 1.** Approximate functions of the normal force in the meshing of the cycloid disc teeth and the ring gear.

| Meshing Type | Approximate Function of the Normal Force for a Single Revolution of the Input Shaft | $F_{\text{low}}$, N | $F_{\text{amp}}$, N |
|---|---|---|---|
| Single tooth meshing | $F(\varphi) = \begin{cases} 0, & [0,20) \\ F_{\text{low}} + \lvert F_{\text{amp}} \cdot \sin(1.5 \cdot \varphi)\rvert, & [20,120] \\ 0, & (120,360] \end{cases}$ | 2387 | 1616.8 |
| Double tooth meshing | $F(\varphi) = \begin{cases} 0, & [0,20) \\ F_{\text{low}} + \lvert F_{\text{amp}} \cdot \sin(2 \cdot \varphi)\rvert, & [20,90] \\ 0, & (90,360] \end{cases}$ | 1530 | 427.7 |
| Triple tooth meshing | $F(\varphi) = \begin{cases} 0, & [0,30) \\ F_{\text{low}} + \lvert F_{\text{amp}} \cdot \sin(1.5 \cdot \varphi)\rvert, & [30,90] \\ 0, & (90,360] \end{cases}$ | 1456 | 293.9 |

Based on the obtained functions given in Table 1, a diagram of the normal force was prepared. The diagram of the normal force $F_n$ as a function of the driving angle $\phi$ is shown in Figure 3.
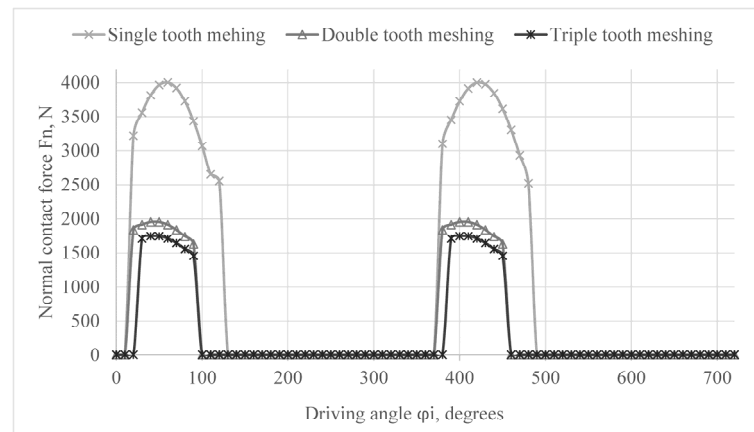
**Figure 3.** Diagram of the normal contact force.

## 3. Experimental Analysis of the Cycloid Disc

The experimental testing was performed at the Center for Engineering Software and Dynamic Testing of the Faculty of Engineering, the University of Kragujevac, on a Shimadzu EHF-EV101KZ-070-0A servo-hydraulic pulsator, with an accuracy of ±0.5% [35]. The test was performed at room temperature (22 ± 2 °C) by controlling the force according to the given input functions (Figure 3). Based on the input forces as a function of the driving angle ϕ (Figure 3), the function was transferred into a time domain corresponding to the rotational speed of the input shaft of the cycloid speed reducer of 350 min$^{-1}$. This was the maximum speed of loading and unloading that could be achieved on the servo-hydraulic pulsator. Higher speeds could not be achieved due to the inertia of the servo-hydraulic pulsator system. The diagram of the input force achieved on the servo-hydraulic pulsator is given in Figure 4.
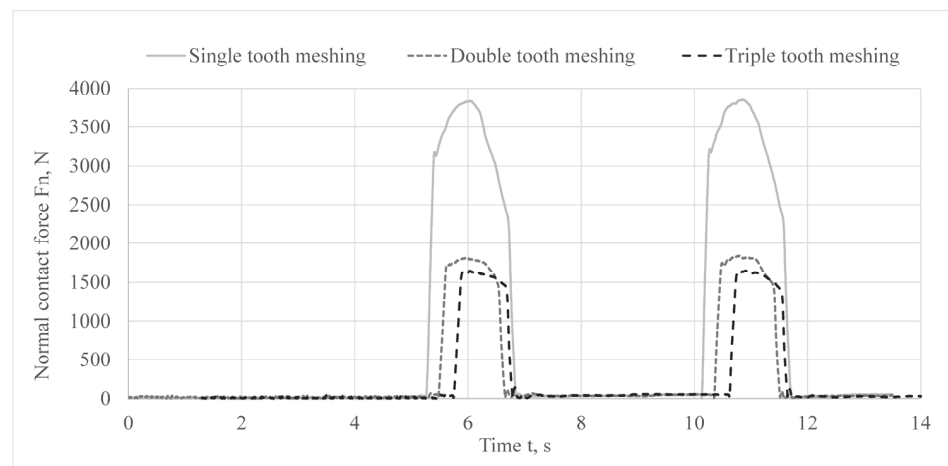


**Figure 4.** The input force achieved at the servo-hydraulic pulsator.

If Figures 3 and 4 are compared, it can be concluded that a precise application of force was achieved using the pulsator. The experimental model on the described pulsator is shown in Figure 5. The direction of eccentricity makes a 20° angle in the horizontal direction. At this position of the eccentric cam, all the elements come into contact, and the compression force assumes a vertical direction. This is a necessary condition for testing on a servo-hydraulic pulsator.

The strain gauge method was used for experimental analysis. Due to space limitations, the strain gauges could not be placed in the contact zone, so they were placed as close to it as possible. We used strain gauge chains 1-KY11-2/120 produced by HBM, one of the world's leading test and measuring equipment manufacturers, with an accuracy of

±1% [36]. Two chains were glued. Each of the glued chains contained 5 strain gauges spaced at 2 mm, which made it possible to measure the strain gradient. The area of a single strain gauge was 1.95 mm$^2$. A schematic presentation of the position of the strain gauges is given in Figure 6.
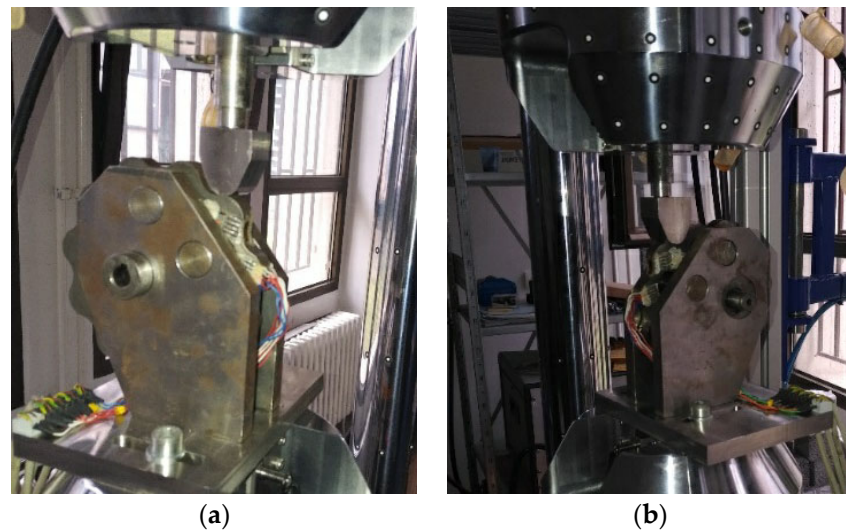


**Figure 5.** The experimental model on the servo-hydraulic pulsator: (**a**) left side view; (**b**) right side view 2.
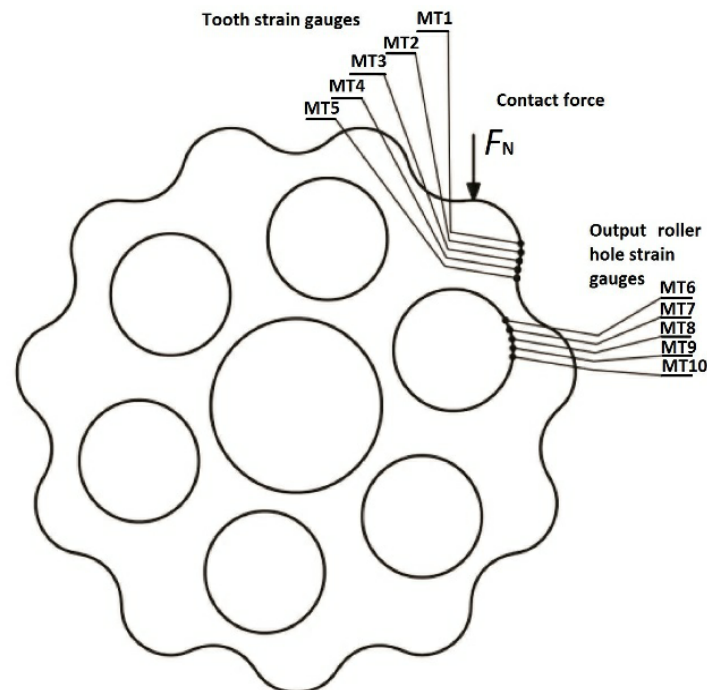


**Figure 6.** Position of the glued strain gauges.

The maximum values given in Table 2 were used to set the maximum compression force. A total of 9 measurements were made for all three meshing cases with load levels of 50%, 100%, and 150% of the force $F_{Nmax}$. The first measurement was made for the case of a triple tooth-meshing of the cycloid disc and a ring gear.
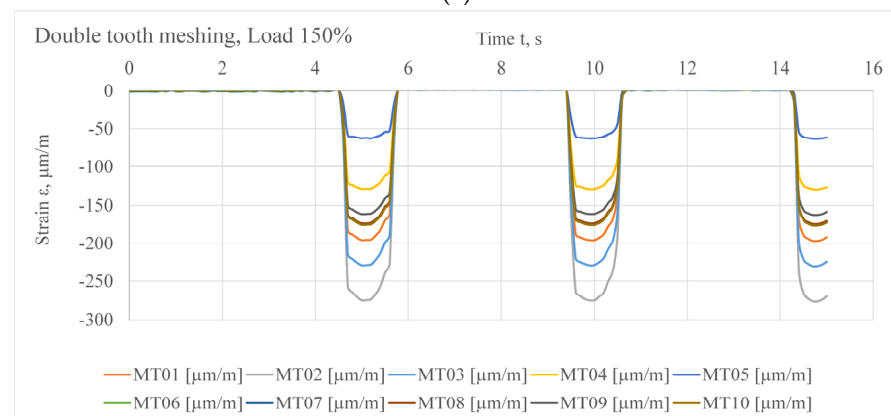
This paper presents strain measurement results for the maximum load of 150% of $F_{Nmax}$. These results are given in Figure 7.
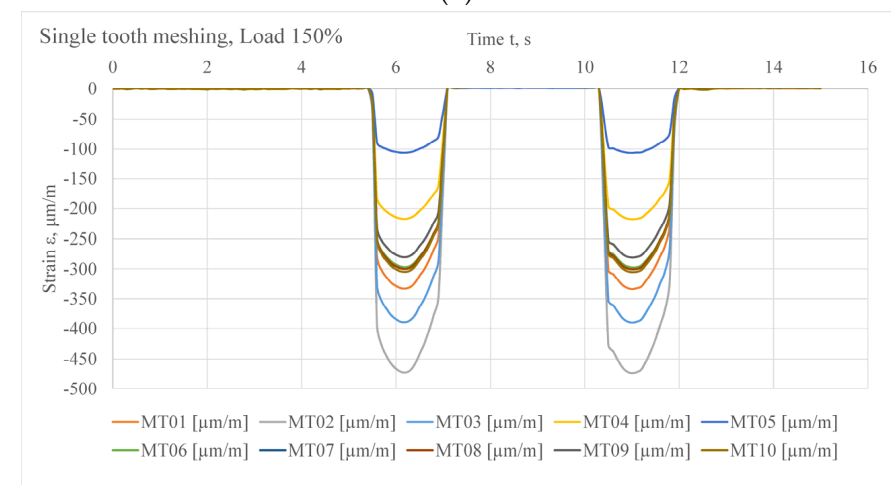
**Table 2.** External loads during the meshing.

| Meshing | Load 50% $F_{\text{Nmax}}$, N | Load 100% $F_{\text{Nmax}}$, N | Load 150% $F_{\text{Nmax}}$, N |
|---|---|---|---|
| Triple tooth | 872.5 | 1745 | 2617.5 |
| Double tooth | 975.5 | 1951 | 2926.5 |
| Single tooth | 2000.5 | 4001 | 6001.5 |
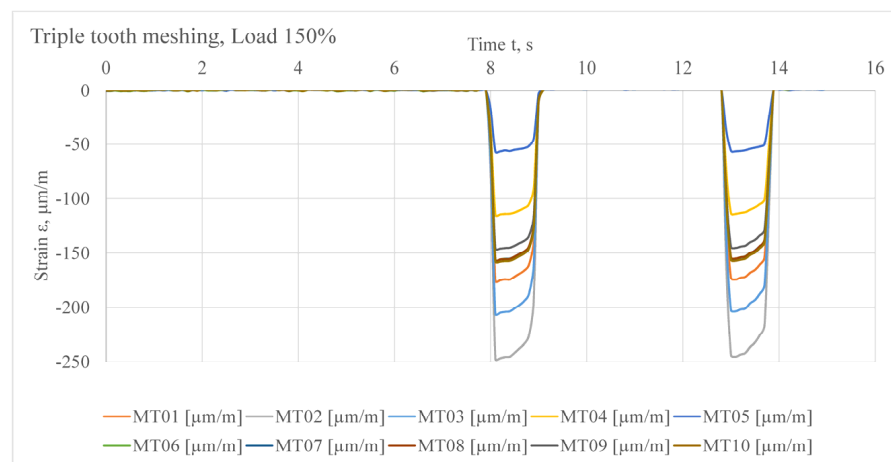


(**a**)



(**b**)



(**c**)

**Figure 7.** Strain results obtained in the time domain for the external load of 150% of $F_{\text{nmax}}$ for: (**a**) triple–tooth meshing, (**b**) double–tooth meshing, and (**c**) single–tooth meshing.

Figure 7, for the load case of 150% of $F_{\text{Nmax}}$, shows the results for three cases of meshing: triple tooth meshing, double tooth meshing, and single tooth meshing. The results present the measured strain by strain gauges. As can be noted, and as well expected, the most critical case is single tooth meshing because the biggest force was applied during that experiment.

## 4. Numerical Analysis of the Stress-Strain State of the Cycloid Disc

In order to verify the performed measurements, numerous numerical analyses were carried out using the finite element method. In both the experimental and numerical analyses for all three types of meshing, loading and unloading were performed to correspond to the actual going of the cycloid disc teeth and the ring gear into and out of the mesh. Namely, the tooth loading was gradually increased until the maximum force was applied, followed by a partial and then a complete tooth unloading until the moment the teeth re-entered the mesh. If Figures 5 and 8 are compared, it can be concluded that the experimental model is very similar to the CAD model used for the numerical analysis so that simulation can follow the experiment procedure.
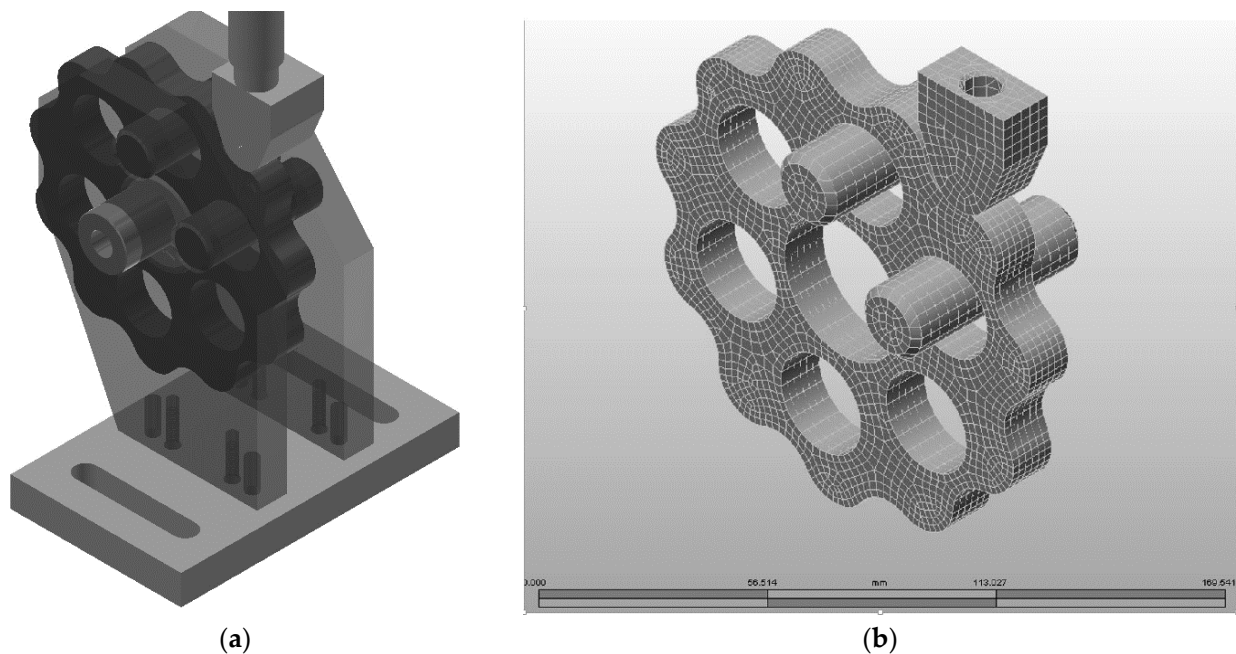


(**a**)                                                                 (**b**)

**Figure 8.** CAD model of a segment of the cycloid speed reducer: (**a**) experimental analysis (**b**) FEM analysis.

The numerical analysis of the stress-strain state of the cycloid disc was performed using the finite element method. The CAD model was made using the Autodesk Inventor software, while the numerical analysis was performed using the Autodesk Simulation Mechanical software, which uses the ALGOR solver. In order to be able to compare the numerical and experimental results, the CAD model for numerical analysis was made based on the physical model of the cycloid disc and other meshing elements used for experimental analysis (Figure 5). For the numerical analysis to be efficient, only the parts in direct contact were considered for the FEA model, while the rest were taken as constraints, Figure 8b.

The numerical analysis was performed as a dynamic analysis in the transient stress environment. Therefore, as part of this dynamic analysis, simulations were performed for a single-tooth, double-tooth, and triple-tooth meshing of the ring gear rollers and cycloid disc teeth. The function of the $F_{\text{Nmax}}$ was modeled in the real-time domain where the loading and unloading correspond to the actual going of the cycloid disc teeth and the ring gear

rollers into and out of the mesh [1,2,30]. The cycloid disc was considered a deformable elastic body in the analyses.

Interactions between the meshed elements were modeled as surface contacts. Unlike in previous studies [30], where the line load was applied in the contact area with the pusher (which simulated the ring gear), the surface contact load transfer was used in this study. As illustrated in Figure 9, the pusher can move only in the vertical direction. In this way, a simulation that most closely represents the operating conditions of the cycloid disc was created. Based on the procedures described in the previous section and in the literature [1,2,30], the force $F_{Nmax}$ was determined for the triple-tooth, double-tooth, and single-tooth meshing. For all three types of meshing, the following external loads were used: 50% of $F_{Nmax}$, 100% of $F_{Nmax}$, and 150% of $F_{Nmax}$. Because of the large number of results obtained, only the results for the dynamic force with the maximum value of 150% of $F_{Nmax}$ modeled for single-tooth, double-tooth, and triple-tooth meshing were presented in the paper.
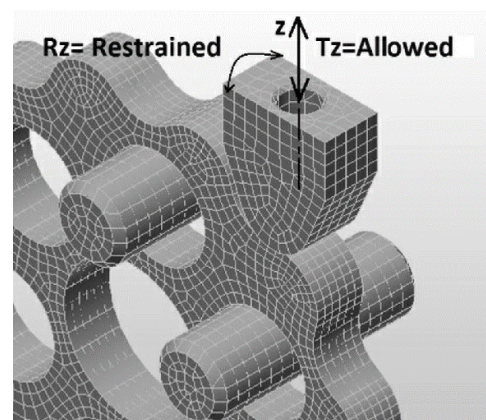


**Figure 9.** Illustration of the limitations of the pusher.

The values of the external loads used in the numerical analysis are given in Table 2. They correspond to the diagram of the forces achieved on the servo-hydraulic pulsator. Table 3 presents the ordinal numbers of the nodes that best correspond to the centers of the strain gauges (Figures 5 and 6). The von Mises stress is chosen for the comparison because it has a similar value to the dominant stress component. The deviation between the dominant stress component and von Mises stress is negligible, which is the main reason for choosing von Misses stress for the comparison of results.

**Table 3.** Comparative presentation of the strain gauges and the corresponding finite element nodes.

| Node Number | MT Number | Node Number | MT Number |
|---|---|---|---|
| Strain von Misses (1377) | MT1 | Strain von Misses (1846) | MT6 |
| Strain von Misses (1378) | MT2 | Strain von Misses (1847) | MT7 |
| Strain von Misses (1379) | MT3 | Strain von Misses (1848) | MT8 |
| Strain von Misses (1380) | MT4 | Strain von Misses (1849) | MT9 |
| Strain von Misses (1381) | MT5 | Strain von Misses (1850) | MT10 |

This problem was regarded as spatial so that the numerical and experimental analyses could be performed with the same boundary conditions. In order to compare the numerical and the experimental results, the strain values were given as a function of time for the positions where the strain gauges were glued in the experimental testing. The positions of the strain gauges are shown in Figure 6—position of the glued strain gauges.

The strain gauges were positioned identically to the ones shown in Figure 6. This was achieved by placing virtual sensors on the nodes of the corresponding finite elements.
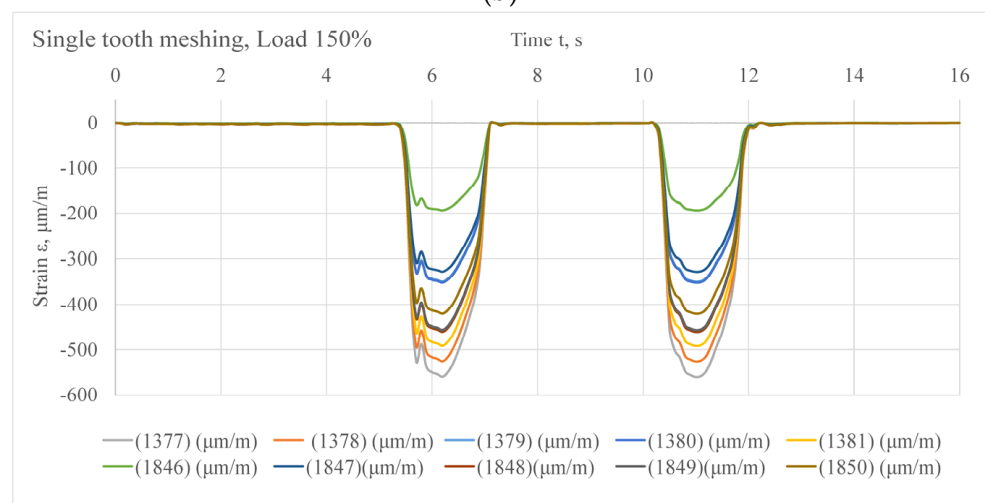
Figure 10 shows the numerical results for all three cases of meshing under the load of 150% of $F_{nmax}$ (Table 2).
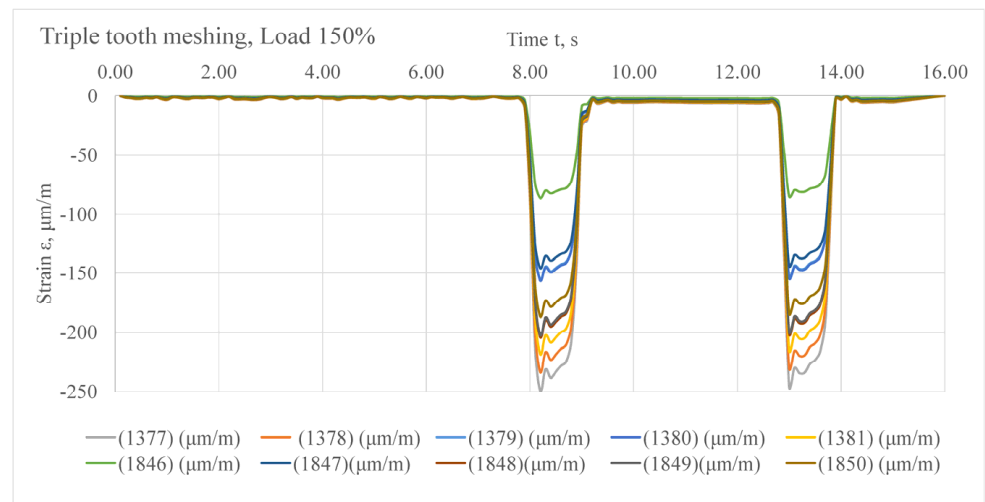


(a)
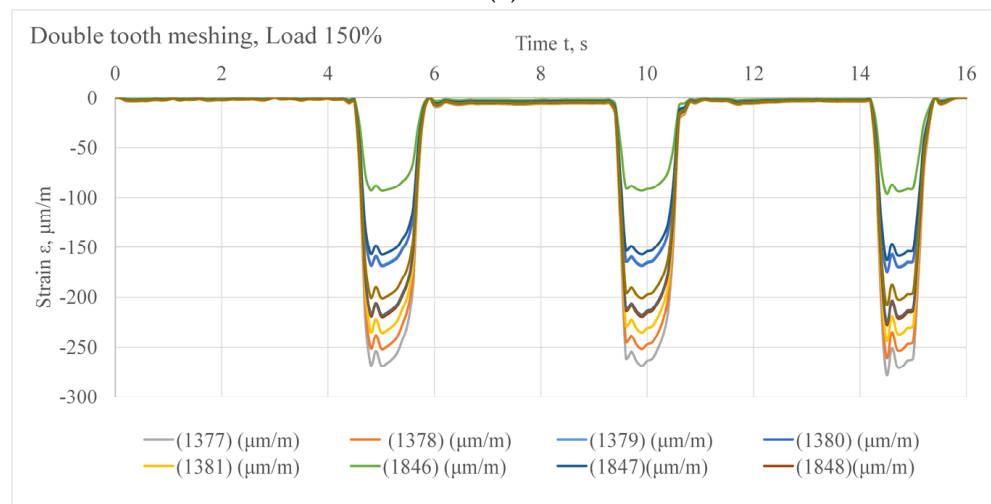


(b)



(c)

**Figure 10.** Von Mises strains in the time domain for the external load of 150% $F_{Nmax}$ for: (**a**) triple–tooth meshing, (**b**) double–tooth meshing, and (**c**) single–tooth meshing.

The cycloid disc was made of steel 30CrMoV9, which for the given thickness, according to the standard EN 10250-3:2000 [37], has a minimum yield stress of $R_e$ = 700 MPa and a minimum tensile strength of $R_m$ = 900 MPa. The other mechanical characteristics of the material needed for the numerical analysis were found in the software library: modulus of elasticity $E = 2.07 \times 10^5$ MPa and Poisson's ratio μ = 0.3.

The lowest stress value on the cycloid disc occurs in the case of the triple-tooth meshing of the cycloid disc and the ring gear (σ = 338 MPa). About 7% higher stresses occur at the double-tooth meshing compared to the triple-tooth meshing, while about 224% higher stresses occur at the single-tooth meshing compared to the triple-tooth meshing. At the single-tooth meshing and the load of 150% of $F_{Nmax}$, the stresses that occur are close to the yield stress value, but this is only for very short time intervals.

According to the literature [23], the stress that occurs in the contact of the cycloid disc and the output rollers can have the most unfavorable effect on the operation of the cycloid speed reducer.

## 5. Experimental and Simulation Results Comparison

A comparative analysis of the numerical and experimental results is presented in this section. Table 4 gives the strain and stress values obtained using the finite element method and experimental testing. The values are given for the force that equals 150% of $F_{Nmax}$ for the most critical moment of loading.
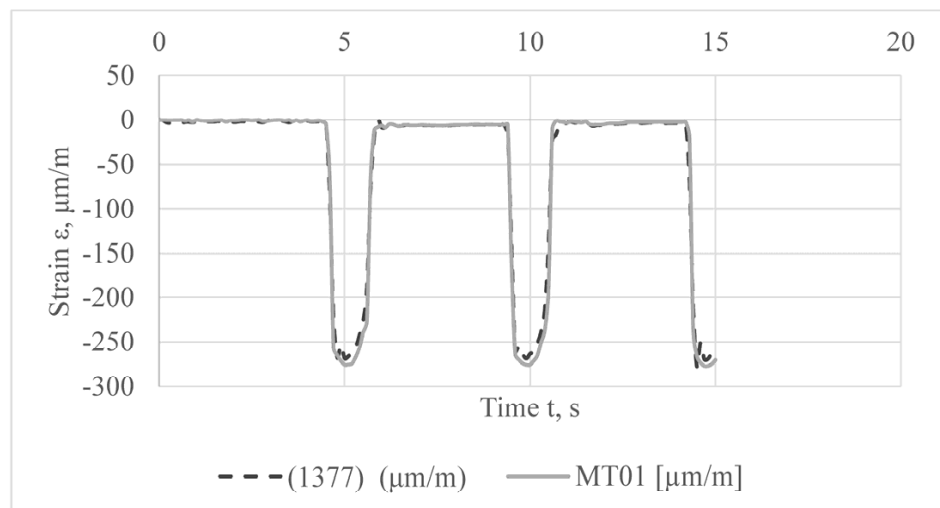
**Table 4.** Comparative results obtained using the finite element method and experimental testing.

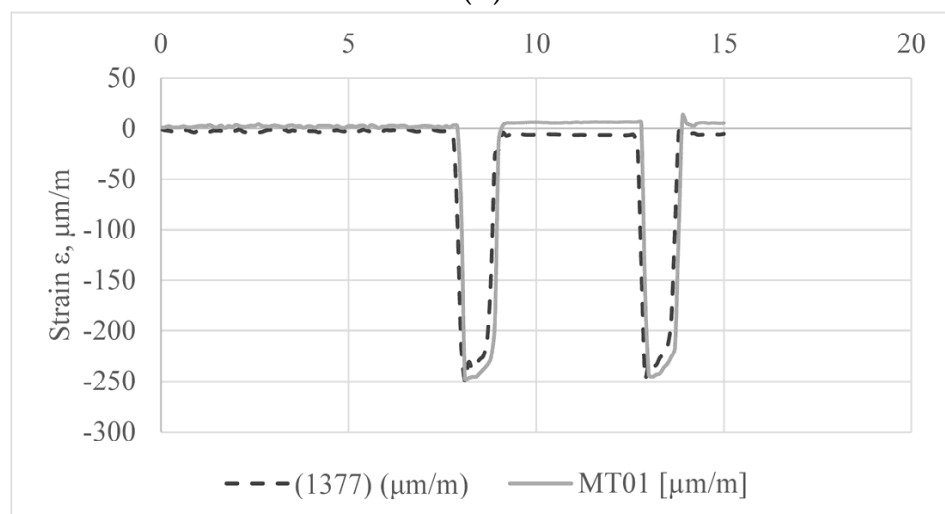| Single-tooth meshing—Load 150% | | | | | | | | | | |
|---|---|---|---|---|---|---|---|---|---|---|
| | MT1 | MT2 | MT3 | MT4 | MT5 | MT6 | MT7 | MT8 | MT9 | MT10 |
| ε—ex., μm m$^{-1}$ | 473.75 | 390.26 | 333.91 | 218.09 | 106.51 | 297.37 | 300.36 | 300.63 | 280.83 | 305.38 |
| σ—ex., MPa | 98.07 | 80.78 | 69.12 | 45.14 | 22.05 | 61.56 | 62.18 | 62.23 | 58.13 | 63.21 |
| ε—num., μm m$^{-1}$ | 561.52 | 526.12 | 491.68 | 352.50 | 350.36 | 193.95 | 328.17 | 459.80 | 455.71 | 420.51 |
| σ—num., MPa | 116.24 | 108.91 | 101.78 | 72.97 | 72.52 | 40.15 | 67.93 | 95.18 | 94.33 | 87.04 |
| Double-tooth meshing—Load 150% | | | | | | | | | | |
| | MT1 | MT2 | MT3 | MT4 | MT5 | MT6 | MT7 | MT8 | MT9 | MT10 |
| ε—ex., μm m$^{-1}$ | 276.69 | 230.16 | 196.74 | 128.87 | 63.27 | 174.69 | 175.92 | 174.99 | 162.58 | 176.74 |
| σ—ex., MPa | 57.28 | 47.64 | 40.73 | 26.68 | 13.10 | 36.16 | 36.42 | 36.22 | 33.65 | 36.59 |
| ε—num., μm m$^{-1}$ | 277.21 | 259.73 | 242.73 | 174.02 | 172.96 | 95.75 | 162.01 | 226.99 | 224.97 | 207.59 |
| σ—num., MPa | 57.38 | 53.76 | 50.25 | 36.02 | 35.80 | 19.82 | 33.54 | 46.99 | 46.57 | 42.97 |
| Triple-tooth meshing—Load 150% | | | | | | | | | | |
| | MT1 | MT2 | MT3 | MT4 | MT5 | MT6 | MT7 | MT8 | MT9 | MT10 |
| ε—ex., μm m$^{-1}$ | 247.28 | 206.24 | 176.15 | 114.69 | 56.69 | 156.37 | 156.53 | 156.46 | 145.70 | 157.98 |
| σ—ex., MPa | 51.19 | 42.69 | 36.46 | 23.74 | 11.73 | 32.37 | 32.40 | 32.39 | 30.16 | 32.70 |
| ε—num., μm m$^{-1}$ | 249.47 | 233.74 | 218.45 | 156.61 | 155.66 | 86.17 | 145.80 | 204.28 | 202.47 | 186.82 |
| σ—num., MPa | 51.64 | 48.39 | 45.22 | 32.42 | 32.22 | 17.84 | 30.18 | 42.29 | 41.91 | 38.67 |

In both numerical and experimental analyses, the highest strain occurs at the site of strain gauge 1, i.e., at the strain von Mises node (1377). Figure 11 shows comparative strain diagrams of strain gauge 1 (MT1) and the corresponding strain von Mises node (1377) for the most unfavorable load when the force $F_N$ reaches 150%.
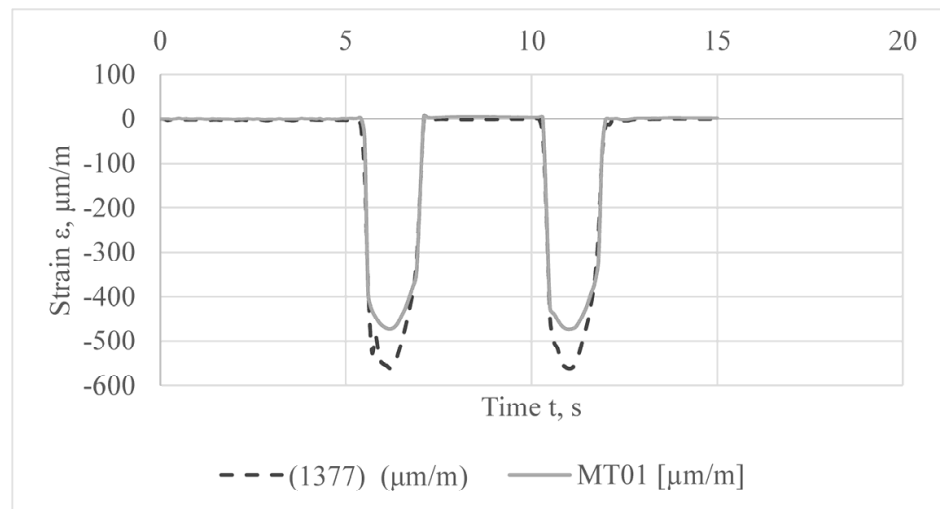
(**a**)



(**b**)



(**c**)

**Figure 11.** A comparative diagram of the numerical and experimental results obtained at site MT1 (node 1377) at the load of 150% of $F_N$ for (**a**) single–tooth meshing; (**b**) double–tooth meshing, and (**c**) triple–tooth meshing.

The stresses that occur in the case of the single-tooth meshing are almost twice as high as that of the double-tooth or triple-tooth meshing of the cycloid disc and the ring gear. This is found in both numerical and experimental analyses. The difference in stresses between the double-tooth and the triple-tooth meshing is much smaller than between the single-tooth and the double-tooth meshing. A correlation analysis was conducted for the presented diagrams. The single tooth meshing results correlates 99.6% between the experimental and numerical results. The double-tooth and triple-tooth meshing results correlate 99.7% and 92.9% between the experimental and numerical results. The biggest deviation in correlation was the triple tooth meshing case because of the multiple meshing contacts and harder input force prediction. The correlation analyses show that the simulation setup follows the experimental procedure in more than acceptable boundaries. The highest stresses occur in the simulations and experiments at the site of strain gauge 1 or node 1377. Figure 11 gives a comparative diagram of the strains at the site of strain gauge 1. Based on Figure 11, it can be concluded that the difference in the strain values is almost negligible in the double-tooth and triple-tooth meshing, while the strain values for the single-tooth meshing differ considerably. Namely, in the case of the triple meshing, the strain values obtained by numerical analysis are slightly lower compared to the values obtained experimentally. The lowest strains occur at the site of strain gauge 5 in the experimental analysis, while in the numerical analysis, the lowest strains occur at strain gauge 6. In the numerical analysis, the strain values are much higher at the sites of strain gauges 4 and 5, while at the site of strain gauge 6, the stress values are lower. This is not the case with other strain gauges. This inconsistency may be caused by improperly glued strain gauges or inhomogeneity of the cycloid disc material, among other reasons. The deviations between the numerical and experimental analysis results for the strain gauge 1 range from 3% to about 15%. Therefore, it can be concluded that the numerical results are valid and that the numerical model was well developed. The deviation between results probably occurred because the von Mises stress is considered instead of the stress component. The results deviation is at appropriate values.

## 6. Conclusions

This paper presents a numerical and experimental dynamic analysis of the stress state of the cycloid disc meshing with other elements of the cycloid speed reducer. A single-tooth, double-tooth, and triple-tooth meshing were analyzed. Based on the obtained results, the following can be concluded:

- There is a high level of matching between the numerical and the experimental results. The level of mismatching for the strain gauge with the largest measured strain, MT1 (node 1377), is between 3% and 15%. This clearly shows that the boundary conditions set for the numerical model corresponded to the operating conditions in the experiment. The presented deviation between the results is in the acceptable interval.
- As expected, the maximum stress occurs in the meshing zone of the cycloid disc and the ring gear. These stress values are far below the material yield stress.
- There are two more places where the stress spikes occur: in the contact area between the cycloid disc and the eccentric cam and in the contact area between the cycloid disc and the output rollers, as shown in [23]. These are expected results, as shown in the literature review.
- The stress values are far below the yield stress value of the cycloid disc material at the double-tooth and triple-tooth meshing, while in the case of the single-tooth meshing, the stress values are close to the yield stress value (the most unfavorable case being when the load was up to 150% of the force $F_{\text{Nmax}}$). Overload is included in this research for the cases of shock forces or increased friction forces occurring during the cycloid drive operation to cover those possibilities as well.
- Based on the performed analysis, it can be concluded that the output rollers of the cycloid speed reducer need to be further studied in more detail since the contact area between the output rollers and the cycloid disc is one of the places where the

highest stresses occur. This is the place that requires further analyses and possible new experimental setups.

- Manufacturing tolerances for cycloid speed reducers should be kept as low as possible, as shown in [21] so that at least a double-tooth meshing can be achieved. This would considerably decrease the stresses occurring during interactions between the elements of the cycloid speed reducer.

In further research, particular attention will be paid to other elements of the cycloid speed reducer, such as the eccentric cam, output rollers, and ring gear.

**Author Contributions:** Conceptualization, M.B. and M.M. (Milos Matejic); methodology, M.M. (Marija Matejic); software, V.M.; validation, V.M. and A.D.; formal analysis, M.M. (Marija Matejic); investigation, A.D.; resources, M.M. (Milos Matejic); data curation, A.D.; writing—original draft preparation, M.M. (Milos Matejic); writing—review and editing, M.B.; visualization, I.M.; supervision, V.M.; project administration, M.B.; funding acquisition, I.M. All authors have read and agreed to the published version of the manuscript.

**Institutional Review Board Statement:** Not applicable.

**Informed Consent Statement:** Informed consent was obtained from all subjects involved in the study.

**Data Availability Statement:** Not applicable.

**Conflicts of Interest:** The authors declare no conflict of interest.

## References

1. Kudrijavcev, V.N. *Planetary Gear Train*; Leningrad: Moscow, Russia, 1966. (In Russian)
2. Lehmann, M. *Calculation and Measurement of Forces Acting on Cycloid Speed Reducer*; Technical University Munich: Munich, Germany, 1976. (In German)
3. Malhotra, S.K.; Parameswaran, M.A. Analysis of a cycloid speed reducer. *Mech. Mach. Theory* **1983**, *18*, 491–499. [CrossRef]
4. Thube, S.V.; Bobak, T.R. *Dynamic Analysis of a Cycloidal Gearbox Using Finite Element Method*; American Gear Manufacturers Association (AGMA): Alexandria, VA, USA, 2012; pp. 241–253.
5. Kniazeva, A.; Goman, A. Definition of a loading zone of a planetary pin reducer eccentric. *Meh. Mashin Meh. I Mater.* **2012**, *3*, 40–52.
6. Wang, S.; Tian, G.; Jiang, X. Estimation of sliding loss in a cycloid gear pair. *Int. J. Adv. Comput. Technol.* **2012**, *4*, 462–469. [CrossRef]
7. Li, S. Design and strength analysis methods of the trochoidal gear reducers. *Mech. Mach. Theory* **2014**, *81*, 140–154. [CrossRef]
8. Hsieh, C.F. Dynamics analysis of cycloidal speed reducers with pinwheel and nonpinwheel designs. *J. Mech. Des. Trans. ASME* **2014**, *136*, 091008. [CrossRef]
9. Hsieh, C.F. The effect on dynamics of using a new transmission design for eccentric speed reducers. *Mech. Mach. Theory* **2014**, *80*, 1–16. [CrossRef]
10. Zhang, L.; Wang, Y.; Wu, K.; Sheng, R.; Huang, Q. Dynamic modeling and vibration characteristics of a two-stage closed-form planetary gear train. *Mech. Mach. Theory* **2016**, *97*, 12–28. [CrossRef]
11. Zhang, F.; Li, P.; Zhu, P.; Yang, X.; Jiang, W. Analysis on dynamic transmission accuracy for RV reducer. *MATEC Web Conf.* **2017**, *100*, 01003. [CrossRef]
12. Ren, Z.Y.; Mao, S.M.; Guo, W.C.; Guo, Z. Tooth modification and dynamic performance of the cycloidal drive. *Mech. Syst. Signal Process.* **2017**, *85*, 857–866. [CrossRef]
13. Song, L.; Shunke, L.; Zheng, Z.; Chen, F. Analysis of the key structures of rv reducer based on finite element method. *IOP Conf. Ser. Mater. Sci. Eng.* **2019**, *544*, 012005. [CrossRef]
14. Bao, H.Y.; Jin, G.H.; Lu, F.X. Nonlinear dynamic analysis of an external gear system with meshing beyond pitch point. *J. Mech. Sci. Technol.* **2020**, *34*, 4951–4963. [CrossRef]
15. Król, R. Resonance phenomenon in the single stage cycloidal gearbox. Analysis of vibrations at the output shaft as a function of the external sleeves stiffness. *Arch. Mech. Eng.* **2021**, *68*, 303–320. [CrossRef]
16. Tsai, Y.T.; Lin, K.H. Dynamic Analysis and Reliability Evaluation for an Eccentric Speed Reducer Based on Fem. *J. Mech.* **2020**, *36*, 395–403. [CrossRef]
17. Tchufistov, E.A.; Tchufistov, O.E. Loading of satellite bearing of planetary cycloid gear by forces acting in meshing. *IOP Conf. Ser. Mater. Sci. Eng.* **2020**, *862*, 032042. [CrossRef]

18. Efremenkov, E.A.; Efremenkova, S.K.; Dyussebayev, I.M. Determination of Geometric Parameter of Cycloidal Transmission from Contact Strength Condition for Design of Heavy Loading Mechanisms. *IOP Conf. Ser. Mater. Sci. Eng.* **2020**, *795*, 012024. [CrossRef]

19. Zhang, T.; Li, X.; Wang, Y.; Sun, L. A semi-analytical load distribution model for cycloid drives with tooth profile and longitudinal modifications. *Appl. Sci.* **2020**, *10*, 4859. [CrossRef]

20. Liu, C.; Shi, W.; Xu, L. A Novel Approach to Calculating the Transmission Accuracy of a Cycloid-Pin Gear Pair Based on Error Tooth Surfaces. *Appl. Sci.* **2021**, *11*, 8671. [CrossRef]

21. Jiang, N.; Wang, S.; Yang, A.; Zhou, W.; Zhang, J. Transmission Efficiency of Cycloid–Pinion System Considering the Assembly Dimensional Chain. *Appl. Sci.* **2022**, *12*, 11917. [CrossRef]

22. Efremenkov, E.A.; Shanin, S.A.; Martyushev, N.V. Development of an Algorithm for Computing the Force and Stress Parameters of a Cycloid Reducer. *Mathematics* **2023**, *11*, 993. [CrossRef]

23. Kumar, N.; Kosse, V.; Oloyede, A. A new method to estimate effective elastic torsional compliance of single-stage Cycloidal. *Mech. Mach. Theory* **2016**, *105*, 185–198. [CrossRef]

24. Chen, C.; Yang, Y. Structural Characteristics of Rotate Vector Reducer Free Vibration. *J. Vibroeng.* **2016**, *18*, 3089–3103. [CrossRef]

25. Yang, Y.H.; Chen, C.; Wang, S.Y. Response sensitivity to design parameters of RV reducer. *Chin. J. Mech. Eng.* **2018**, *31*, 49. [CrossRef]

26. Lin, T.C.; Schabacker, M.; Ho, Y.L.; Kuo, T.C.; Tsay, D.M. Geometric Design and Dynamic Analysis of a Compact Cam Reducer. *Machines* **2022**, *10*, 955. [CrossRef]

27. Blagojević, M. Stress and Strain State of Cycloreducer's Elements under Dynamic Loads. Ph.D. Thesis, University of Kragujevac, Faculty of Mechanical Engineering, Kragujevac, Serbia, 2008.

28. Blagojevic, M.; Nikolic-Stanojevic, V.; Marjanovic, N.; Veljovic, L. Analysis of Cycloid Drive Dynamic Behavior. *Sci. Tech. Rev.* **2009**, *59*, 52–56.

29. Blagojevic, M.; Marjanovic, N.; Djordjevic, Z.; Stojanovic, B.; Disic, A. A new design of a two-stage cycloidal speed reducer. *J. Mech. Des. Trans. ASME* **2011**, *133*, 085001. [CrossRef]

30. Blagojevic, M.; Marjanovic, N.; Djordjevic, Z.; Stojanovic, B.; Marjanovic, V.; Vujanac, R.; Disic, A. Numerical and experimental analysis of the cycloid disc stress state. *Teh. Vjesn.* **2014**, *21*, 377–382.

31. Blagojevic, M.; Matejic, M. Stress and strain state of cycloid gear under dynamic loads. *Mach. Des.* **2016**, *8*, 129–132.

32. Blagojević, M.; Matejić, M.; Kostić, N. Dynamic behaviour of a two-stage cycloidal speed reducer of a new design concept. *Teh. Vjesn.* **2018**, *25*, 291–298. [CrossRef]

33. Blagojevic, M.; Matejic, M.; Vasic, M. Comparative Overview of Calculation of Normal Force on Cycloidal Gear Tooth. In Proceedings of the International Congress Motor Vehicles & Motors—Conference Porceedings, Kragujevac, Serbia, 9 October 2020; University of Kragujevac, Faculty of Engineering: Kragujevac, Serbia, 2020; pp. 131–137.

34. Blagojevic, M.; Kocic, M.; Marjanovic, N.; Stojanovic, B.; Dordevic, Z.; Ivanov; Marjanovic, V. Influence of the Friction on the Cycloidal Speed Reducer Efficeicncy. *J. Balk. Tribol. Assoc.* **2012**, *18*, 217–227.

35. SHIMADZU Dynamic and Fatigue Testing Systems Your Partner for Dynamic and Fatigue Tests. Shimadzu Cat. 2021. Available online: https://www.ssi.shimadzu.com/products/materials-testing/fatigue-testing-impact-testing/index.html (accessed on 20 February 2023).

36. HBM Strain Gauges: Absolute Precision from HBM. Straing Gauges Accessories Cat. 2014. Available online: https://www.straingauges.cl/images/blog/catalogo%20de%20strain%20gages.pdf (accessed on 15 January 2023).

37. *EN 10250-3:2000*; Open Steel Die Forgings for General Engineering Purposes Alloy Special Steels. British Standards Institution: London, UK, 1999.